Logical OR operation and magnetic field sensing based on layered topology

Junyang Sui[1], Dan Zhang[3] and Haifeng Zhang[2,*] [iD]

[1] School of Materials Science and Engineering, Nanjing University of Posts and Telecommunications, Nanjing 210023, People's Republic of China
[2] College of Electronic and Optical Engineering & College of Flexible Electronics (Future Technology), Nanjing University of Posts and Telecommunications, Nanjing 210023, People's Republic of China
[3] College of Information Science and Technology, Nanjing Forestry University, Nanjing 210026, People's Republic of China

E-mail: hanlor@163.com

CrossMark

Abstract

A one-dimensional magnetized InSb photonic crystals layered topology (PCLT) proposed in this paper can realize the functions of logic OR operation and magnetic field sensing. In the proposed PCLT, under the transverse magnetic polarization, the value and frequency of the absorption peak (AP) can be controlled by the external magnetic fields and has a high-quality factor (Q), thus OR logical operation can be achieved. Additionally, since InSb has a magneto-optical effect under magnetic fields, the parity of the structure of the PCLT which adds InSb as defect layers can be broken. Electromagnetic waves obtain nonreciprocity when propagating in opposite directions within the PCLT, which means that logical operation and magnetic field sensing based on AP can be obtained on the forward and backward scales. For the detection, on the forward scale, optimum performances of Q, sensitivity (S), the figure of merit, and detection limit are 62 372.09, 0.0169 $(2\pi c/d)/T$, 4225 T^{-1}, 1.2×10^{-5} T, and for the backward detection, the corresponding values are 63 626.25, 0.0225 $(2\pi c/d)/T$, 5200 T^{-1}, 1×10^{-5} T. The designed PCLT is innovative in multi-functional and multi-scale, having certain research value and prospects.

Keywords: logical operation, photonic structure, detection, nonreciprocity

(Some figures may appear in colour only in the online journal)

1. Introduction

Logic gates based on the photonic crystals layered topology (PCLT) have been widely studied in recent years, it is an important branch of the integrated optical path, and there are many applications in the fields of optical sensing, optical communications, such as optical signal processors [1], photonic microprocessors [2] and optical instruments. An important part of implementing logic gates is the PCLT. PCLT is arranged periodically by different refractive index media, which can be divided into one-dimensional (1D), two-dimensional (2-D) [3], and three-dimensional arrangements [4]. In general, because 1D PCLT has photonic band gaps (PBGs) [5], the electromagnetic waves (EWs) cannot propagate in the PBGs under normal conditions [6]. But numerous studies have shown that [7, 8], under the condition of introducing appropriate defect layers, a passband at a specific frequency is created in the PBGs, in which EWs can propagate. This feature provides ideas for the implementation of logical operations.

It is known that InSb owns a magneto-optical effect under the action of an applied magnetic field [9], and this effect can make changes in the dielectric constants due to the free carriers

of InSb [10]. Therefore, magnetic field sensing can be realized via a magnetic field controlling the dielectric constants of the PCLT. With the deepening of research, different types of magnetic field sensors have been designed, such as eddy current sensors [11], fluxgate magnetic sensors [12], and induction coil magnetic sensors [13]. They play a huge role in the field of information science.

Nonreciprocity is widely served in sensors [14], optical diodes [15], and isolators [16], and it refers to EWs propagating in opposite directions with different EWs loss and phase shift [17]. The nonreciprocity of EWs propagation can be generated when EWs propagate in the opposite direction within the structure whose cosmology is broken [18, 19]. The 1D PCLT proposed is asymmetrical, contributing to realizing the nonreciprocity. Additionally, due to InSb owning the high electron mobility, under relatively small magnetic fields, it will show the gyrotropy property near the cyclotron frequency located in the terahertz (THz) state [20] which can lead to nonreciprocity. Furthermore, due to the introduction of the magnetic InSb, the magneto-optical effect which can break the parity of the PCLT can also help to enhance the nonreciprocity [21]. Thus EWs can propagate nonreciprocally within the PCLT. Here, we can use the strength of the nonreciprocity EWs propagation to equip the 1D PCLT device with two measurement scales.

With the rapid progress of research, devices that can be used for magnetic field sensing and logical gates have been extensively studied. Chen *et al* [22] proposed a high-fidelity frequency-encoded deterministic two-photon controlled-phase gate which could be achieved via exploiting the strong photon–photon correlation enabled by photonic dimers and the unique nonreciprocal photonic propagation in chiral quantum nanophotonic systems. Yan *et al* [23] used two large photonic crystals ring resonators, one small ring resonator, and the photonic crystals branch waveguides to design a 2D PCLT THz wave logic AND–XOR gate which also owned small sizes and was simple to fabricate. Wu *et al* [24] investigated optical logic gates with good *S* based on the phase control which cloud be observed in photonic crystals heterostructures and asymmetric defective photonic crystals. These devices have very good performance parameters, but it exists a pity that the devices investigated only can realize a single function such as sensing or logic gates. In recent years, a device owning multi-function and multi-scale forms a new direction of research. Zhuo *et al* [25] designed a photodetector that integration of the monolayer graphene onto the side-polished optical fiber, combining the functions of photodetection and optical phase modulation. Badri *et al* [26] proposed a reconfigurable optical bandpass filter based on subwavelength grating (SWG), and could also be used as a nonvolatile optical switch due to tuning the resonance wavelength and transmission peak. Badri *et al* [27] demonstrated an optical filter based on a silicon SWG waveguide evanescently coupled to phase-change material loading segments arranged periodically around the SWG core. Moreover, a switching functionality with an extinction ratio of 28.8 dB was added to the structure due to employing the phase-change material $Ge_2Sb_2Te_5$. Youngblood *et al* [28] produced a single

graphene-based device that can simultaneously provide efficient optical modulation and photodetection. These results broaden the research ideas of related fields. Therefore, the electromagnetic devices own the functions of both logic gates and sensing detectors having great research potential.

In this paper, we study a 1D PCLT that can implement both logic OR operations and magnetic field sensing functions, which makes innovation and breakthrough in previous studies. Specifically, OR logic operations modulated by magnetic fields are implemented. On this basis, by locating the absorption peak (AP), a detector with a high-quality factor (*Q*) value, high *S*, high figure of merit (FOM) and low detection limit (DL) for measuring weak magnetic field changes can be successfully realized. In addition, the nonreciprocity created by the introduction of magnetized InSb as defect layers means logic operations and detection that can be done simultaneously on both forward and backward scales. Furthermore, in several cases of OR logical operations, the linear equations have different *Q* values, detection ranges, and *S* when EWs propagate respectively forward and backward, which is the bright spot in the paper. It should be stressed that this paper is mainly theoretical research, and experiments are not included in the scope of this work.

2. Theoretical model and simulation

The 1D magnetized InSb PCLT we designed is shown in figure 1(a), it is formed by a quasi-periodic asymmetric arrangement of an ordinary dielectric. InSb is added as a defect layer and its optical rotation effect under the external magnetic fields increases the time inversion and spatial asymmetry of the structure. For the universality of the structure, PCLT will be exposed to air. Under the transverse electric (TE) mode, distributed only on the transverse plane perpendicular to the direction of propagation are the electric field components. Conversely, the magnetic field components only exist in the transverse plane perpendicular to the propagation direction in the occurrence of the transverse magnetic (TM) polarization [29]. Here, we only focus on the TM mode, and the external magnetic fields are B_1 and B_2, which are parallel to the $-y$ axis and are respectively applied to $InSb_1$ and $InSb_2$. The angle of incidence is θ which refers to the angle between the EWs and the *z*-axis, where the incidence of EWs are positive angles. When EWs propagate in the 1D magnetized InSb PCLT, the Lorentz force affects the EWs due to the TM polarization, while the TE polarization does not. Therefore, the effects of the TM polarization can be controlled by the external magnetic field [30]. The incidence paths of EWs during the forward and backward propagation are indicated by blue and red arrows, respectively. Given the universality of the results, the normalized thickness is set as *d*. The common dielectrics are indicated by A, B, C, D, E, F, G. And d_A, d_B, d_C, d_D, d_E, d_F, and d_G are used to simplify the thickness of these dielectrics. By normalizing the thickness of the medium, the incident frequency of EWs can be normalized to $\omega = 2\pi c/d$, and here we set $2\pi c/d$ as α. This structure defines the thickness of each media layer as $d_A = 0.6d$, $d_B = 0.4d$, $d_C = 0.75d$,
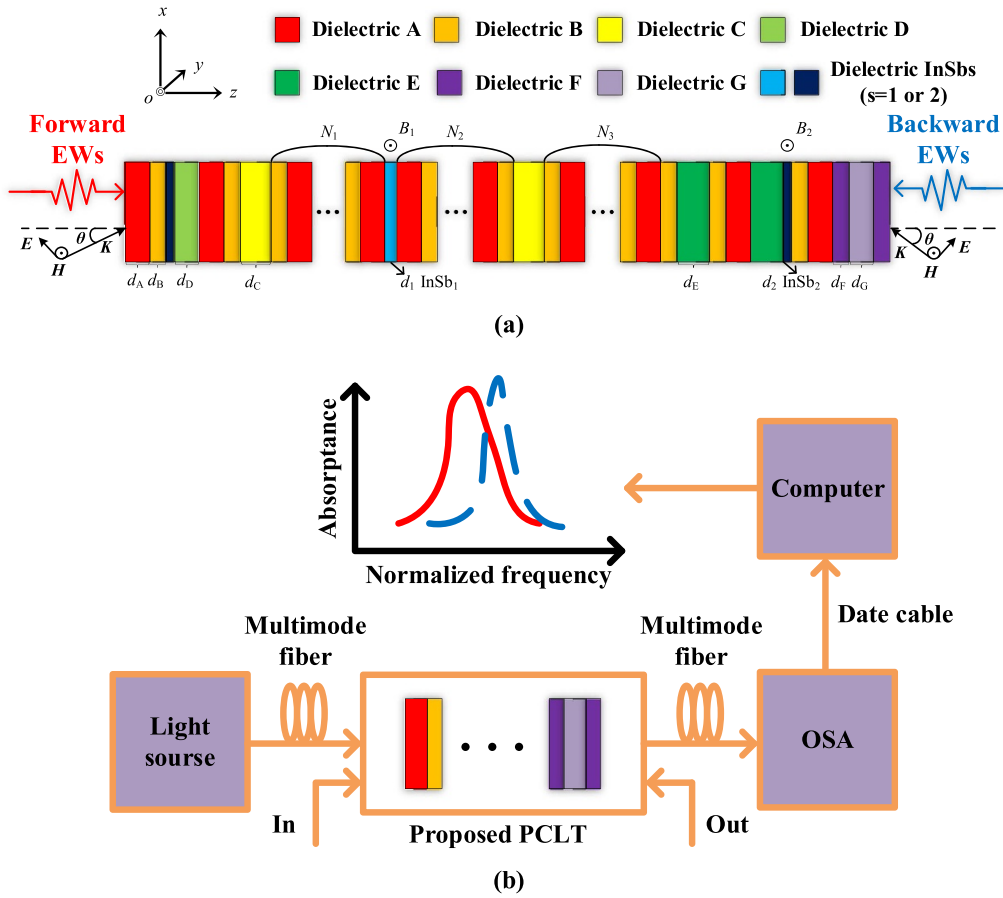
Figure 1. (a) The schematic structure of magnetized InSb 1D PCLT. (b) The setup configuration of the experiment probes the absorption.

$d_D = 0.6d$, $d_E = 0.8d$, $d_F = 0.4d$ and $d_G = 0.6d$. The thicknesses of the two semiconductors InSb$_1$ and InSb$_2$ are fixed at $d_1 = 0.069d$ and $d_2 = 0.05d$. Figure 1(a) shows the entire structure, where the filter structure is the structure 'GFG'. The numbers of the omitted period are severally about $N_1 = 10$, $N_2 = 14$, and $N_3 = 7$. The refractive indexes of the dielectrics are set to $n_A = 2.391$, $n_B = 1.697$, $n_C = 2.371$, $n_D = 2.86$, $n_E = 1.8$, $n_F = 3.87$, and $n_G = 3.97$. In addition, the transfer matrix method is used to analyze the entire structure [31, 32].

Under the condition of the external magnetic fields applied to the layers of InSb, the dielectric of InSb exhibits an anisotropic tensor, and its dielectric function is described as [33]:

$$\varepsilon_{\mathbf{Insb}} = \begin{bmatrix} \varepsilon_x & 0 & \varepsilon_{xz} \\ 0 & \varepsilon_y & 0 \\ -\varepsilon_{xz} & 0 & \varepsilon_x \end{bmatrix}, \tag{1}$$

in which, the matrix elements as [33]:

$$\varepsilon_x = \varepsilon_\infty - \varepsilon_\infty \frac{\omega_p^2 (\omega + i\nu_c)}{\omega \left[(\omega + i\nu_c)^2 - \omega_c^2 \right]}, \tag{2a}$$

$$\varepsilon_y = \varepsilon_\infty - \varepsilon_\infty \frac{\omega_p^2}{\omega(\omega + i\nu_c)}, \tag{2b}$$

$$\varepsilon_{xz} = \varepsilon_\infty \frac{i\omega_p^2 \omega_c}{\omega \left[(\omega + i\nu_c)^2 - \omega_c^2 \right]} \tag{2c}$$

where the angular frequency is expressed in ω and normalized to α. By using the appropriate unit thickness d, we can take d as an appropriate cell thickness to gain the EWs in the THz. Here, the high-frequency limit permittivity, collision frequency, and plasma frequency of the carrier are respectively indicated by ε_∞, ν_c, and ω_p. Here $\varepsilon_\infty = 15.68$ [34], $\omega_p = Ne^2/\varepsilon_0 m^*$, N is the intrinsic carrier concentration, equation (3) list the expression, ε_0, and e respectively represent the dielectric constant and electron charge in the vacuum, the effective mass of the carrier is indicated by m^*. The electron mass m_e is related to m^*, $m^* = 0.015m_e$ for InSb [33]. ν_{c1} and ν_{c2} represent the carrier collision frequencies in two different InSbs, where $\nu_{c1} = 0.00006\omega_p$ and $\nu_{c2} = 0.000008\omega_p$. $\omega_c = eB/m^*$ symbolizes the electron gyration frequency. Through magnetic fields regulation, in order to accurately realize the logic OR function on the forward and backward scales, and keep the sharp AP generated by different OR logic conditions in the same scale at the same frequency point, after parameter optimization, the values of magnetic fields B_1 and B_2 respectively corresponding to forward and backward scales are different. For the forward propagation, initially, $B_1 = 1.36$ T and $B_2 = 1.14$ T. Similarly, $B_1 = 1.411$ T and $B_2 = 1.407$ T when the EWs propagate in the opposite direction. What needs illustration is that our work

studies the theoretical model, ordinary dielectrics are not influenced by an external magnetic field, and the thicknesses of InSb layers are very thin compared to ordinary dielectric layers, so the magnetic field applied to the particular InSb layer is in a small area, other InSb layers not affected. If considering the experimental application, Xuan *et al* [35] designed a gradient magnetic field coil. By applying current to it, a spatial linear magnetic field can be generated, which meets the requirements of this paper that the magnetic field sizes on different InSb layers are different and the influences of adjacent magnetic fields can be isolated.

In addition, the effect of N on the dielectric properties of InSb is crucial, which greatly depends on T_0. T_0 is the temperature, and it takes 270 K, which follows the equation as [33]:

$$N(m^{-3}) = 5.76 \times 10^{20} T_0^{1.5} \\ \times \exp\left[-0.26/(2 \times 8.625 \times 10^{-5} \times T_0)\right]. \quad (3)$$

The Effective permittivity for InSb materials under TM polarization can be worked out as [36]:

$$\varepsilon_{\text{TM}} = \frac{\varepsilon_x^2 - \varepsilon_{xz}^2}{\varepsilon_x^2}, \quad (4)$$

according to the $\varepsilon_x = \varepsilon_\infty - \varepsilon_\infty \frac{m^{*2}\omega_p^2(\omega + i\nu_c)}{\omega[m^{*2}(\omega + i\nu_c)^2 - e^2 B^2]}$ and $\varepsilon_{xz} = \varepsilon_\infty \frac{im^*\omega_p^2 eB}{\omega[m^{*2}(\omega + i\nu_c)^2 - e^2 B^2]}$, ε_x and ε_{xz} change as the size of B changes, but ε_y will not. Therefore, the three tensors in the dielectric function of InSb will have different values, becoming asymmetric tensors. When InSb layers are introduced into PCLT, the nonreciprocity will increase. The size of ε_{TM} is influenced by the magnetic strength B. In addition, the refractive index is $n_{\text{TM}} = (\varepsilon_{\text{TM}})^{1/2}$.

To highlight the contribution of the three tensors in the InSb dielectric function to anisotropy under TM polarization, the dielectric function of InSb under TE wave propagation is given here. since there is no magnetic field applied ($B = 0$ T) under TE polarization, the matrix elements indicate that $\varepsilon_x = \varepsilon_y$, $\varepsilon_{xz} = 0$, so the dielectric constant of InSb is isotropic. The effective dielectric function for InSb can be followed as:

$$\varepsilon_{\text{TE}} = \varepsilon_x = \varepsilon_\infty - \varepsilon_\infty \frac{\omega_p^2}{\omega(\omega + i\nu_c)}. \quad (5)$$

Obviously, its value is independent of the magnetic field strength B. The refractive index under TE polarization is $n_{\text{TE}} = (\varepsilon_{\text{TE}})^{1/2}$.

Under the TM polarization, the transfer matrix is expressed as [35]:

$$M_{\text{TM}} = \begin{bmatrix} \cos(k_{iz}d_i) + \frac{k_{ix}\varepsilon_{xz}}{k_{iz}\varepsilon_x}\sin(k_{iz}d_i) & -\frac{i}{\eta_i}\left[1 + \left(\frac{k_{ix}\varepsilon_{xz}}{k_{iz}\varepsilon_x}\right)^2\right]\sin(k_{iz}d_i) \\ -i\eta_i\sin(k_{iz}d_i) & \cos(k_{iz}d_i) - \frac{k_{ix}\varepsilon_{xz}}{k_{iz}\varepsilon_x}\sin(k_{iz}d_i) \end{bmatrix}, \quad (6)$$

where k_x and k_z are the inverse components of the wave vector on the x- and z-axes, respectively. InSb$_1$ and InSb$_2$ are described by i denoting 1 or 2, respectively, where $k_x = n_{\text{TM}}\sin\theta_i\omega/c\cdot$, $k_z = n_{\text{TM}}\cos\theta_i\omega/c$, here c refers to the speed of light in a vacuum. The optical admittance is indicated by $\eta_i = (\varepsilon_0/\mu_0)n_{\text{TM}}/\cos\theta_i$, here μ_0 is the permeability of a vacuum.

In addition, with j to describe different materials, the dielectric A, B, C, D, E, F, G can be indicated by j, the transfer matrix of its dielectric is shown below [36], written as:

$$M_j = \begin{bmatrix} \cos(k_{jz}d_j) & -\frac{i}{\eta_j}\sin(k_{jz}d_j) \\ -i\eta_j\sin(k_{jz}d_j) & \cos(k_{jz}d_j) \end{bmatrix}, \quad (7)$$

where $k_{jz} = \sin\theta_j\omega/c$. Due to the magneto-optical effect and asymmetric arrangement, EWs correspond to different transmission matrices in the forward and backward propagation, respectively, realizing nonreciprocity. Making M_f the forward propagation and M_b the backward propagation. The entire transfer matrix of the forward and backward propagation can be represented as follows.

We dived the entire transfer matrix of the forward propagation into two parts. The front part M_1 as:

$$M_1 = (M_A M_B M_{TM_2} M_D (M_A M_B) M_C (M_A M_B) \\ \times M_C (M_B M_A)^{10} M_{TM1} (M_A M_B)^{14}, \quad (8)$$

and the latter part M_2 expressed as:

$$M_2 = M_C (M_B M_A)^7 M_B M_E (M_B M_A) M_E M_{TM2} (M_B M_A) M_F M_G M_F, \quad (9)$$

so the entire transfer matrix of the forward propagation Mf is given as:

$$M_f = M_1 M_2. \quad (10)$$

Similarly, the front part of the entire backward transfer matrix M3 shows as:

$$M_3 = M_F M_G M_F (M_A M_B) M_{TM2} M_E (M_A M_B) M_E M_B \\ \times (M_A M_B)^7 M_C, \quad (11)$$

and the second part M4 indicated as:

$$M_4 = (M_B M_A)^{14} M_{TM1} (M_A M_B)^{10} M_C (M_B M_A) M_D M_{TM2} \\ \times (M_B M_A), \quad (12)$$

so the enter transfer matrix of the backward propagation Mb is gained as:

$$M_b = M_3 M_4 \qquad (13)$$

where M_{TM1} and M_{TM2} are the transport matrices of InSb$_1$ and InSb$_2$ materials, respectively, with the expression equation (6). The transmission matrices of dielectrics A, B, C, D, E, F, G are indicated by M_A, M_B, M_C, M_D, M_E, M_F and M_G with the specific expression equation (7).

The reflection and transmission coefficients are calculated as [29]:

$$r = \frac{(m_{11} + m_{12}\eta_{N+1})\eta_0 - (m_{11} + m_{12}\eta_{N+1})}{(m_{11} + m_{12}\eta_{N+1})\eta_0 + (m_{11} + m_{12}\eta_{N+1})}, \qquad (14)$$

$$t = \frac{2\eta_0}{(m_{11} + m_{12}\eta_{N+1})\eta_0 + (m_{11} + m_{12}\eta_{N+1})}, \qquad (15)$$

where $\eta_0 = \eta_{N+1} = (\varepsilon_0/\mu_0)^{1/2}n_0/\cos\theta_0$, the calculation formulas for reflectance and transmittance are displayed as [36]:

$$R = |r|^2, \qquad (16)$$

$$T = |t|^2. \qquad (17)$$

Many studies have shown that the absorption rate in experiments is affected by many factors. For example, an exact dissipation model applying to correlated photon transport in waveguide QED systems is proposed and indicates that a reduced Hamiltonian and a restricted eigen-state can explain the photon leakages to the scattering channels, resulting in atomic dissipation [37]. Moreover, the effects of reservoir-induced dissipation for an arbitrary photonic Fock state transport in waveguide quantum electrodynamic (wQED) are also investigated [38]. However, our work is based on the ideal model without considering the influence of these factors. Hence, the formula for calculating the rate of absorption is obtained as [34]:

$$A = 1 - R - T. \qquad (18)$$

Figure 1(b) shows the experimental setup configuration used to measure absorption. The configuration mainly consists of an optical tunable source (OTS), designed PCLT structure, optical spectrum analyzer (OSA), and computer. Between OTS and the designed structure, and between the designed structure and OTS, multimode optical fibers are used to connect. OTS is connected to the computer by a data cable. When the signal is input from left to PCLT and output from the right. The specific signal transmission and absorption rate measurement process are as follows: The signal is output from OTS, transmits through a multimode fiber, and enters the PCLT structure from the left end. After the structure, the signal is output from the right end and input to the OSA through the multimode fiber. At this point, the computer connected to the OSA can obtain the corresponding spectrum, which can be analyzed to measure the absorption rate in the optical band.

3. Analysis and discussion

The article below will carry out a more explicit functional analysis. Figure 2 shows the absorption spectra of the forward and backward propagation magnetic control logic operation. We can use target AP to detect different physical quantities.

The input logic level (LL) is represented by the different strengths of the two external magnetic fields. The first input is the external magnetic field strength B_1, and the second input is the strength of B_2. The input LL '1' symbolizes that it exists a magnetic field that is applied to InSb, otherwise the LL '0' will display on the input. At the same time, the output is the LL '1' when the absorptance (A) is more than 0.9, and A under 0.2 symbolizes the output LL '0', the precise magnetic field modulation logic OR operation function is formed by these.

As shown in figure 2(a), when EWs propagate forward, A is much less than 0.1 when neither the B_1 nor the B_2 is added to the structure. Figures 2(b)–(d) present that, when EWs propagate forward, only one magnetic field B_1 or B_2 is present, both B_1 and B_2 exist, and sharp AP (A is more than 0.9) is generated, and the corresponding normalized angular frequency (NAF) point of the AP is very close. Figures 2(e)–(h) demonstrate that, when propagating in the backward direction, the results produced by the AP are similar to those produced by the forward propagation, except that the angular frequency points corresponding to the AP produced by the forward and backward propagation are significantly different. That is when any input behaves as LL '1', the LL of '1' must display on the output, as the same as the logic operations '1 OR 0 = 1', '0 OR 1 = 1' and '1 OR 1 = 1', respectively. Conversely, when all inputs are represented as LL '0', the output will be regarded as the LL '0', corresponding to the logic operation '0 OR 0 = 0'. These phenomena clearly express logic OR operations. For a more intuitive exhibition, 'In$_1$' and 'In$_2$' are used for the first input and the second input, respectively, and 'Ou$_1$' for the output. The multi-layer topology structure designed in this paper is arranged by precise calculation and parameter optimization. It can form sharp AP after the InSb layer is introduced, and maintain good nonreciprocity in the forward and backward direction by using the optical rotation effect of InSb. Figures 2(i) and (j) demonstrate that when the InSb layers are removed, no sharp AP is formed in the forward and backward range and the nonreciprocity is very poor. Table 1 shows the truth value table of the OR logical operations.

In addition, for the forward logic operations, when B_1 exists and B_2 does not, $f = 0.2495\,\alpha$ is the corresponding NAF point of the AP, with a Q value of 9242.04 and an absorption rate of 0.9538. When B_2 exists and B_1 does not, the frequency point of the AP is $f = 0.2495\,\alpha$, and the corresponding values of Q and A are respectively about 62 372.5 and 0.9317. When both B_1 and B_2 exist, the NAF point is $f = 0.2495\,\alpha$. 62 372 and 0.9538 are the values of Q and A. Similarly, for the backward logic operations, $f = 0.2546\,\alpha$, $Q = 7957.22$ and A is 0.9638. When B_2 exists and B_1 does not, $f = 0.2546\,\alpha$, $Q = 50\,928.4$ and A is 0.9471. Under the condition of both B_1 and B_2 exist, $f = 0.2546\,\alpha$, $Q = 50\,928.8$ and A is 0.9529. This means that the logic OR operations of different frequencies can be

J. Phys. D: Appl. Phys. **55** (2022) 415001
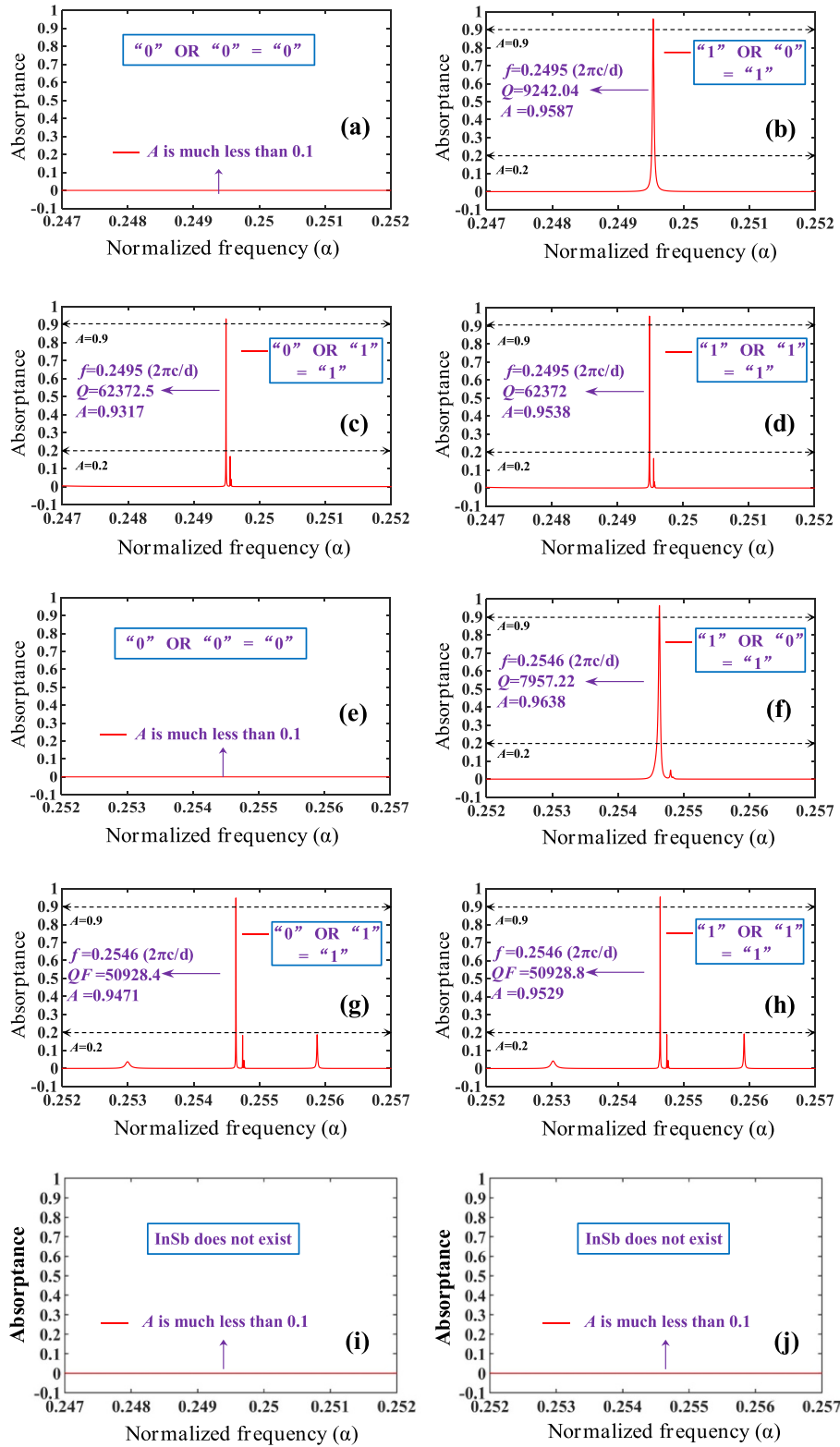
J Sui *et al*

Figure 2. Schematic diagrams of magnetic-controlled logic OR operations and AP when EWs propagate. The forward logic OR operation and corresponding AP under magnetic control: (a) neither B_1 nor B_2 exists. (b) Only B_1 exists. (c) Only B_2 exists. (d) Both B_1 and B_2 exist. The backward logic OR operation and corresponding AP under magnetic control: (e) neither B_1 nor B_2 exists. (f) Only B_1 exists. (g) Only B_2 exists. (h) Both B_1 and B_2 exist. When InSb layers do not exist: (i) the forward diagram of A. (j) The backward diagram of A.

J. Phys. D: Appl. Phys. **55** (2022) 415001

J Sui *et al*

Table 1. Truth value table belongs to the OR logic operations (the parentheses show the performance of input and output).

In_1	In_2	Ou_1
0	0	0
$1(B_1$ exists)	0	$1(A > 0.9)$
0	$1(B_2$ exists)	$1(A > 0.9)$
$1(B_1$ exists)	$1(B_2$ exists)	$1(A > 0.9)$

realized on the forward scale and backward scale, and different Q values can be obtained. Additionally, weak fluctuations in external magnetic fields can be detected by the device. When only B_1 or B_2 exists, both B_1 and B_2 exist, the LL displays on the output as '1' and sharp AP will generate. So, we can position the target AP to realize the detection function of the high Q value of the AP spectrum.

To explain the formation causes of the target resonant AP with different positions of the PCLT when the EWs respectively propagate forward and backward, figure 3 shows the simulation plot of the electric field energy distribution is given when the frequency of EWs in the range of 7.48 THz to 7.64 THz. Here, we set d as 10 μm. It should be noted that because there are too many layers of the PCLT and the electric field energy is concentrated in the first half of the incident light propagation direction, for the sake of the observation, we divide the PCLT into two parts and present one of the parts when EWs propagate on both forward and backward scales. Figures 3(a)–(c) are the left half part of the PCLT. They illustrate that under forward propagation, only B_1 or B_2 exists, both B_1 and B_2 exist, and the electric field energy suddenly increases as EWs pass through the InSb$_2$ layer. Figures 3(d)–(f) present the right half part of the PCLT. Where figure 3(d) shows that, under the condition that only B_1 exists, the energy of the electric field is greatly enhanced between the first layers of InSb$_2$ and the layer of InSb$_1$ when EWs propagate in the backward direction. Figures 3(e) and (f) display that under the backward propagation, as EWs pass through the InSb$_2$ layer, the energy of the electric field is sharply enhanced in the case of only B_2 exists, both B_1 and B_2 exist. Because the layers of defect gather the energy of the electric field, the electric field strength will increase dramatically in this layer. Forward EWs and reflected EWs work with each other in the defect layer, resulting in a phase-canceling interference effect, and the amplitude of the electric field is thus enhanced. In addition, cavity resonance is formed due to the introduction of defects, so that the energy is superimposed in the defect layer, and the sharp resonance AP is thus generated. The result indicates that on the forward and backward scales, due to magnetic structures and asymmetrical structures, resonances can be excited at different positions of the PCLT, showing nonreciprocity.

When we fix one of the external magnetic fields applied to the layers of InSb, the other external magnetic field can be detected by 1D magnetized InSb PCLT, and good logic OR operation can be maintained within the detection range, in particular, this function can be kept at different linear intervals on the forward and backward scales. Because the A of AP is much

less than 0.2 when neither B_1 nor B_2 exists, corresponding to the logic OR operation '0 OR 0 = 0', we can not realize magnetic field sensing via locating sharp AP ($A > 0.9$), here we do not discuss this case.

Figure 4 indicates that when the strength of B_2 is fixed, the target AP will move with the strength of B_1 and the NAF point. Figure 4(a) shows that for the forward detection, under the condition of $B_2 = 0$ T, the continuous AP shows an excellent linear relationship and the A is more than 0.9 in this range when the B_1 is in the range of 1.19 T to 1.4 T. Similarly, figure 4(b) depicts that under backward detection, B_1 within the scope of 1.403 T to 1.411 T indicates a fairly good linear relationship when $B_2 = 0$ T, and A exceeds 0.9 in this range. The accurate magnetic field detection based on the target sharp AP position can be achieved. At the same time, B_1 exists and B_2 does not, which symbolizes the corresponding LL of '$In_1 = 1$' and '$In_2 = 0$' displayed on the input, and the LL of the output will indicate '$Ou_1 = 1$' as A is greater than 0.9.

Figures 5(a) and (b) appear the linear fitting relationship (LFR) between the B_1 and the NAF to further analyze the performance of detection. For the forward detection, under the condition of $B_2 = 0$ T, the LFR of B_1 is $f = 0.0115B_1 + 0.233\,89$ in which the B_1 ranges from 1.19 T to 1.4 T. 0.0115 α/T is the S which can also be calculated as 2.17 THz T^{-1} (d is set to 10 μm), and the range of 0.247 56 α to 0.249 99 α is the NAF of B_1. Linearity can be reflected by the value of R-squared. The higher the R-squared value is, the higher the fitting degree is and the higher the reliability of the trend line is. Due to the R-square being 0.9995, the changes of AP own superb linearity. Under the backward detection, when $B_2 = 0$ T, the LFR is $f = 0.0225B_1 + 0.222\,94$ from 1.403 T to 1.411 T, and the R-square is 0.9995 symbolizing good linearity. The S of the LFR is 0.0225 α/T which is also described as 4.24 THz T^{-1} and the NAF of B_1 is in the range of 0.254 45 α to 0.254 63 α, which is different from the forward detection. FOM, Q, and DL are the critical parameters to evaluate the performance of magnetic field detection. An excellent sensor has high S, FOM, Q, and low DL. The S is higher means that FOM is higher, and ultimately the wavelength resolution is higher. The FOM is defined and evaluated for sensing, which is calculated by equation (19):

$$FOM = \frac{S}{FWHM}, \tag{19}$$

where the half-height width (FWHM) implies the half-height width of the resonant peak [39]. Figure 6 shows the values of Q and FOM for forward and backward sensing of B_1 when the B_2 remains 0 T. Under the condition of the forward sensing, the average values of FOM, Q, and DL are about 482.09 T^{-1}, 10 425.24, 1.06 $\times$ 10^{-4} T, respectively, and the average value of the AP is 0.9514, exceeding 0.9, ensuring output LL $''O_1 = 1''$. Reverse sensing average values are about 682.684 T^{-1}, 7723.76, 0.76 $\times$ 10^{-4} T. The average value of the AP is 0.9422 during backward sensing, which is greater than the absorption rate during forwarding sensing.

Figure 7 is the *x-y* plane view of the successive AP under the condition of the B_2 existing and B_1 changing. On the basis
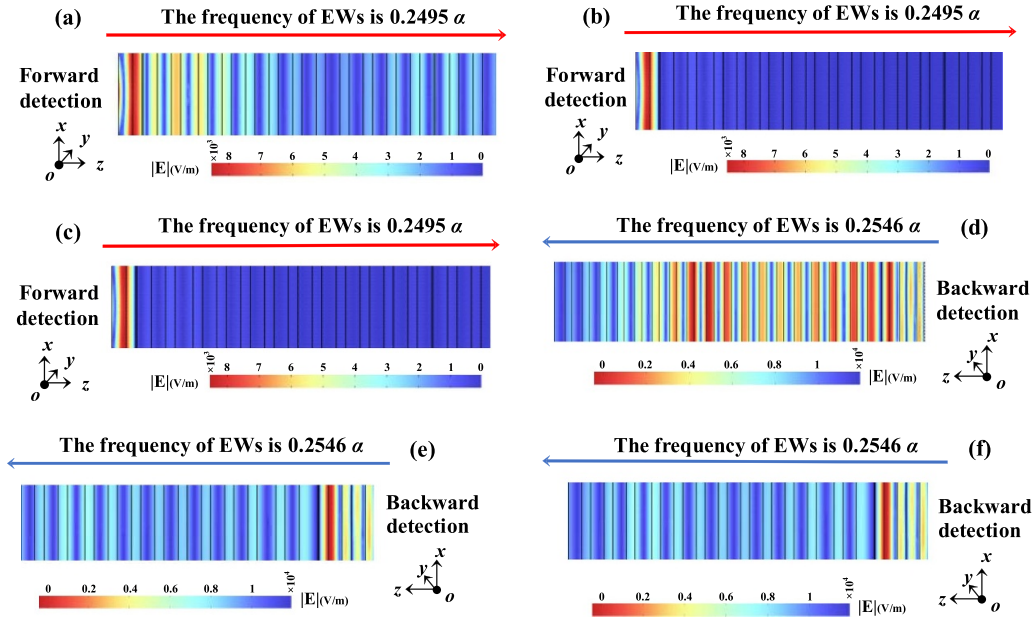
Figure 3. The simulation diagrams of the electric field energy distribution. The left half structure simulation diagram when $f = 0.2495\ \alpha$ under EWs propagating on the forward scale: (a) B_1 exists and B_2 does not. (b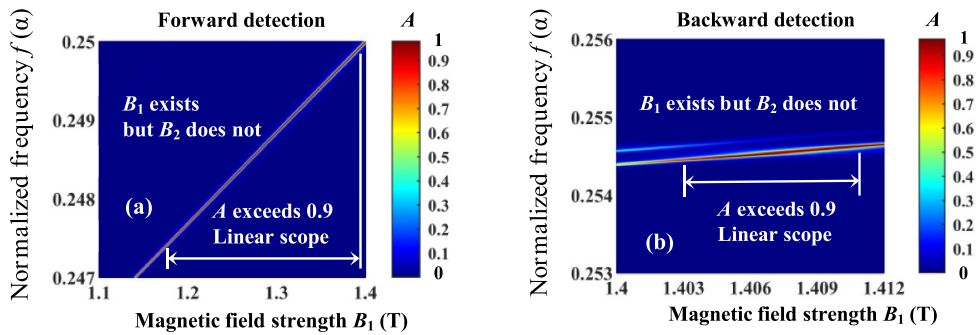) B_2 exists and B_1 does not. (c) Both B_1 and B_2 exist. The right half structure simulation diagrams when $f = 0.2546\ \alpha$ under EWs propagating on the backward scale: (d) B_1 exists and B_2 does not. (e) B_2 exists and B_1 does not. (f) Both B_1 and B_2 exist.

Figure 4. The top view of A which varies with the magnetic field strength B_1 used for detection and the NAF, where B_1 exists and B_2 does not: (a) changes in the A of forward propagation. (b) Changes in the A of backward propagation.
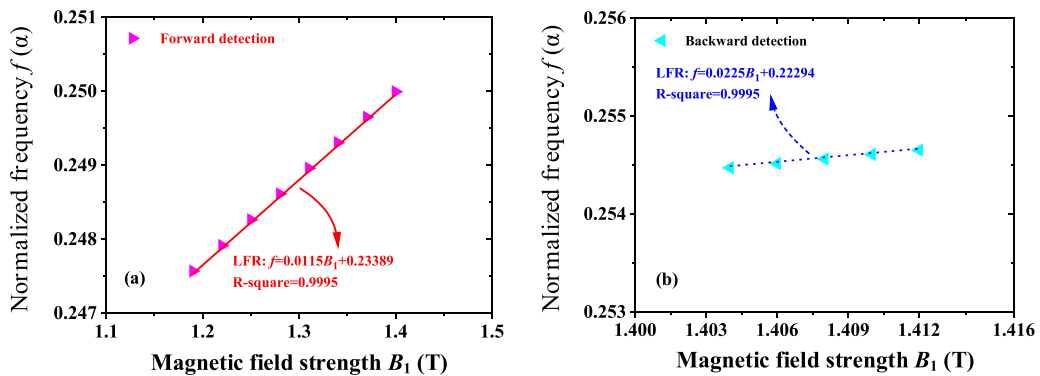
Figure 5. LFR between NAF and magnetic field strength B_1 on the forward and backward sales when B_1 exists and B_2 does not. (a) The forward scale. (b) The backward scale.

of A surpassing 0.9, figure 7(a) shows that when EWs propagate on a forward scale, the B_1 changes in the interval of 1.358 T to 1.37 T based on $B_2 = 1.14$ T. And for the backward detection, figure 7(b) indicates that B_1 is in the range of 1.405 T

to 1.411 T when the $B_2 = 1.407$ T. Figure 8(a) shows the LFR severally belongs to forward and backward detection. $f = 1.11 \times 10^{-4}B_1 + 0.249\ 31$ is the LFR under the forward detection. The S is $1.11 \times 10^{-4}\ \alpha/T$ whose specific
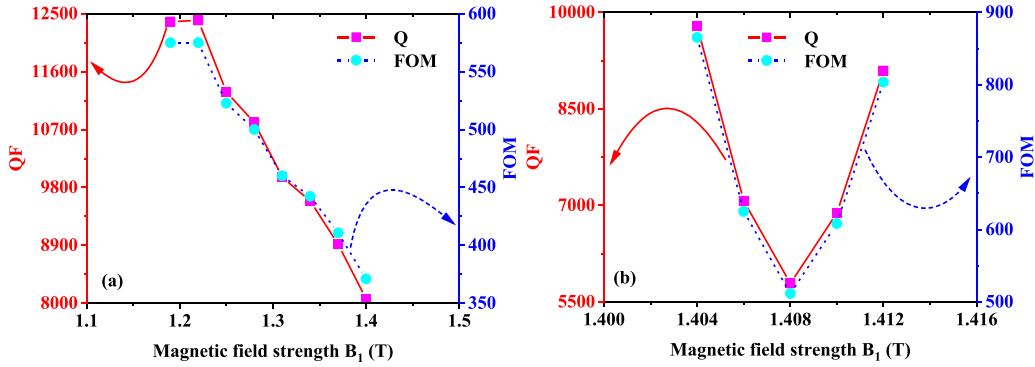
J. Phys. D: Appl. Phys. **55** (2022) 415001

J Sui *et al*

Figure 6. The Q and FOM at different B_1 under the condition of '1 OR 0 = 1'. (a) The forward sensing. (b) The backward sensing.
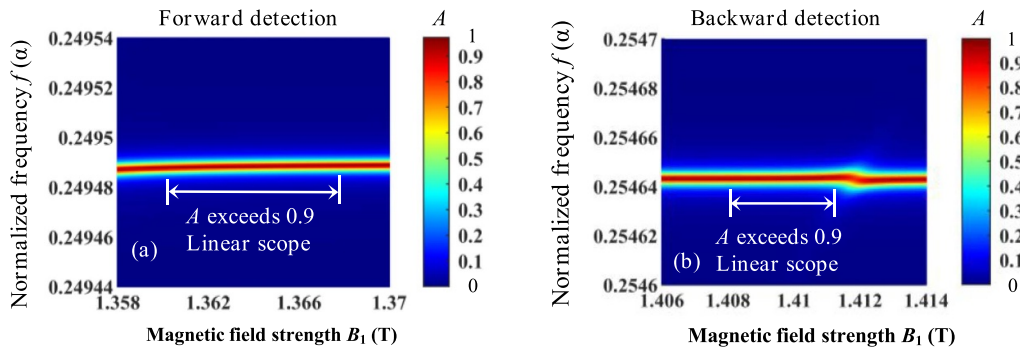

Figure 7. The top view of A which varies with the magnetic field strength B_1 used for detection and the NAF, where both B_1 and B_2 exist; (a) changes in the A of forward propagation. (b) Changes in the A of backward propagation.
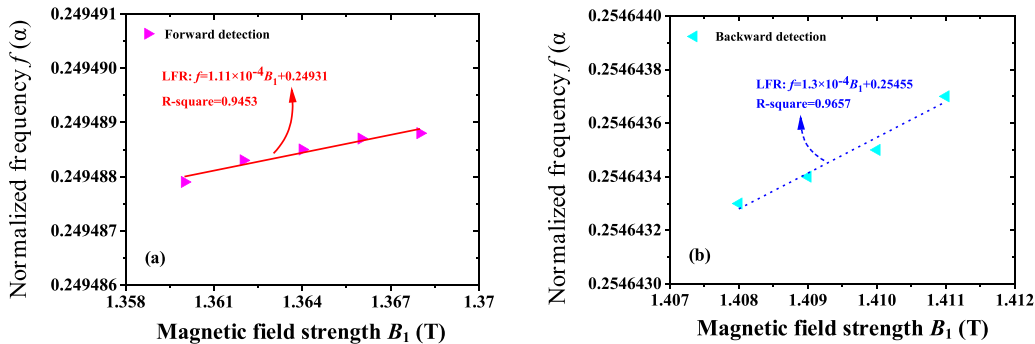

Figure 8. LFR between NAF and magnetic field strength B_1 on the forward and backward sales when both B_1 and B_2 exist. (a) The forward scale. (b) The backward scale.

value is 2.09×10^{-2} THz T^{-1}, and the NAF of B_1 is in the range of 0.249 487 α to 0.249 489 α. The R-square of the LFR is 0.9453, which means the linearity is relatively general. For the backward detection, (see figure 8(b)) the LFR is $f = 1.3 \times 10^{-4} B_1 + 0.254\ 55$, $8.33 \times 10^{-5}\ \alpha$/T is the S, and the range of NAF is from 0.254 643 α to 0.254 644 α. Hence, the specific S is 2.45×10^{-2} THz T^{-1} and R-square is equal to 0.9657. Figure 9(a) points out that for the forward detection when the B_2 is maintained at 1.14 T, the average sizes of FOM, Q, and DL are respectively about 33.25 T^{-1}, 62 372.09, 15.04×10^{-4} T, and the average value of AP is 0.9518, more than 0.9. Under the condition of B_2 remaining at 1.407 T, the reverse detection average values presented in figure 9(b) are about 26 T^{-1}, 50 928.7, and 19.23×10^{-4} T. The average A

is 0.9824 in the context of backward detection, ensuring the output is LL 'Ou$_1 = 1$'. Since the B_1 continuously changes and B_2 always keeps a fixed value, so the LL 'In$_1 = 1$' and LL 'In$_2 = 1$' are displayed on the input.

In figures 10(a) and (b), in the case of $B_1 = 0$ T, the ranges of B_2 from 1 T to 1.2 T and 1.34 T to 1.46 T are individually corresponding to forward and backward detection, and the values of AP keep more than 0.9. Therefore, the precise detection based on the target AP position can be achieved. Simultaneously, B_2 exists and B_1 does not, which symbolizes the corresponding LL 'In$_2 = 1$' and LL 'In$_1 = 0$'. And the LL is 'Ou$_1 = 1$' displayed on the output as the A exceeding 0.9. In order to gain the S of the detection, the LFR between B_2 and the NAF is plotted in figure 11. On the
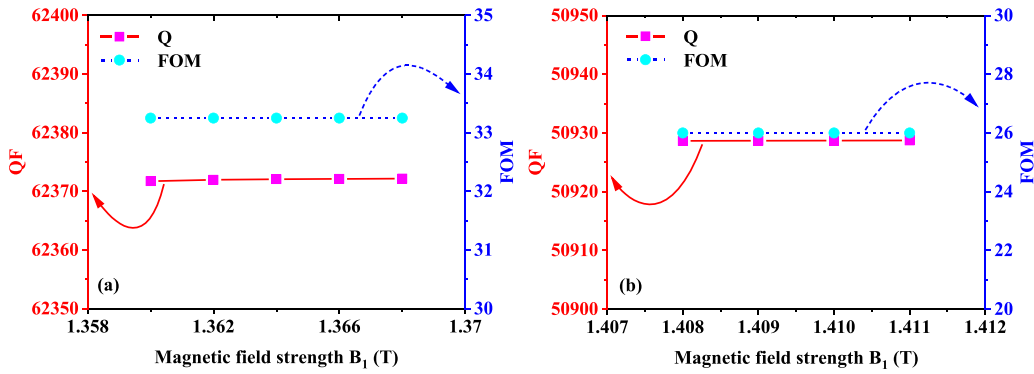
Figure 9. The Q and FOM at different B_1 under the condition of '1 OR 1 = 1'. (a) The forward sensing. (b) The backward sensing.
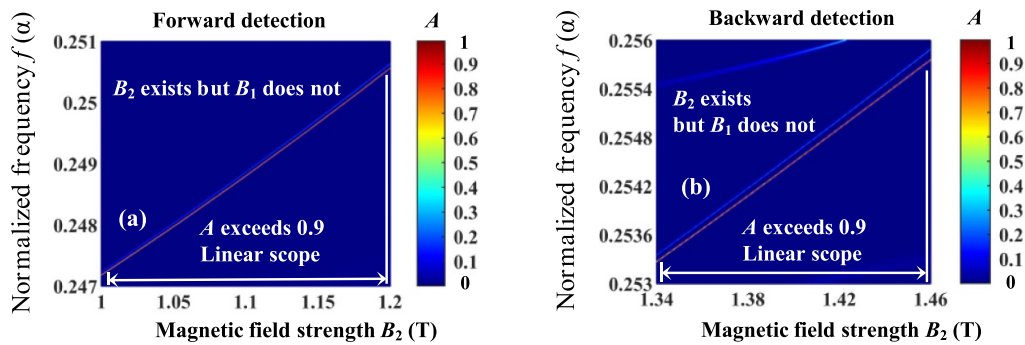

Figure 10. The top view of A which varies with the magnetic field strength B_2 used for detection and the NAF, where B_2 exists and B_1 does not: (a) changes in the A of forward propagation. (b) Changes in the A of backward propagation.
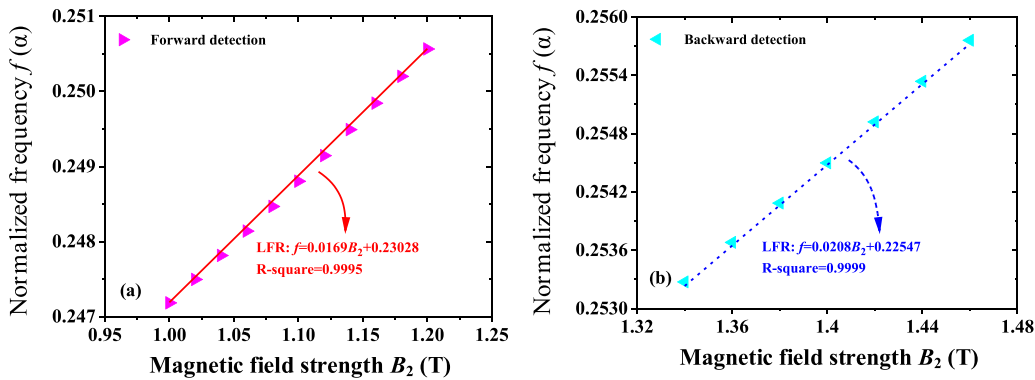

Figure 11. LFR between NAF and magnetic field strength B_2 on the forward and backward sales when B_2 exists and B_1 does not. (a) The forward scale. (b) The backward scale.

basis of maintaining $B_1 = 0$ T, $f = 0.0169B_2 + 0.23028$ and $f = 0.0208B_2 + 0.225\,47$ are severally the LFR of B_2 when detecting magnetic field on forward and backward scales. From the LFR, for sensing forward, the S is 0.0169 α/T and the NAF of B_2 is in the interval of 0.247\,18 α to 0.250\,56 α. Hence, the specific S can be calculated as 3.19 THz T^{-1} when the d is set to 10 μm and R-square is 0.9995 which symbolizes nice linearity. On the other hand, the S is 0.0208 α/T and 0.253\,27 α to 0.255\,76 α is the NAF, R-square of the LFR is 0.9999. Average values of FOM, Q, and DL for forward and backward sensing of B_2 when the B_1 remains at 0 T are indicated in figure 12. Under the situation of forwarding

detection, 4225 T^{-1}, 62\,208.79, 0.12 $\times$ 10^{-4} T are the top values of FOM, Q, and DL, and 0.9501 is the mean value of AP, ensuring output LL $''$Ou$_1$ = 1$''$. Under the negative direction of detection, optical values are about 5200 T^{-1}, 63\,626.25, 0.1 $\times$ 10^{-4} T. Average A is 0.9643, which makes certain output LL $''$1$''$.

When taking B_1 as a fixed strength, the proposed PCLT can detect the magnetic field intensity of B_2. The logic OR operation can also realize in the range of B_2 and satisfy '1 OR 1 = 1'. To get the aim of simplification, shown in figure 13(a), for the forward detection, the B_2 changes from 1 T to 1.14 T, and the corresponding NAF is from 0.247\,18 α to 0.249\,49 α when
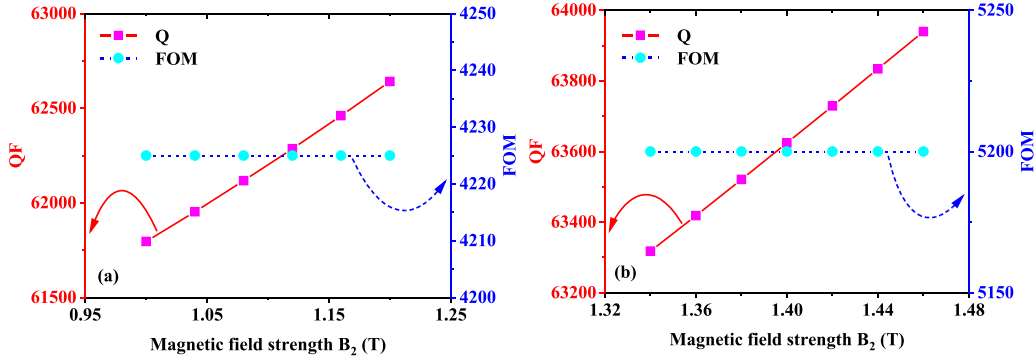
Figure 12. The Q and FOM at different B_2 under the condition of '0 OR 1 = 1'. (a) The forward sensing. (b) The backward sensing.
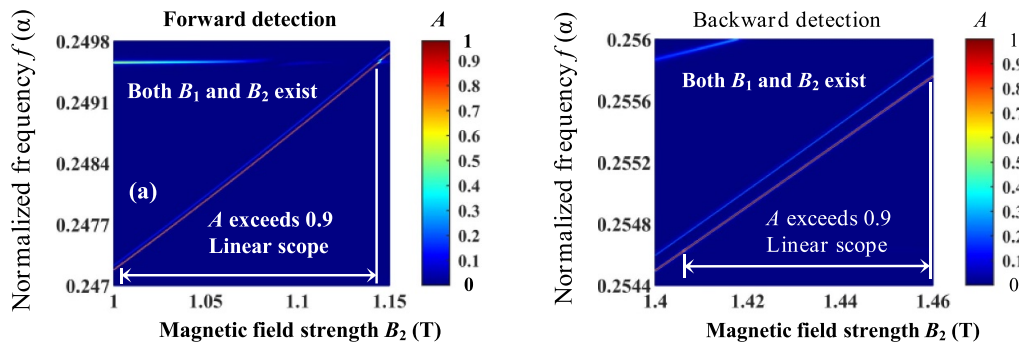

Figure 13. The top view of A which varies with the magnetic field strength B_2 used for detection and the NAF, where both B_1 and B_2 exist: (a) changes in the A of forward propagation. (b) Changes in the A of backward propagation.
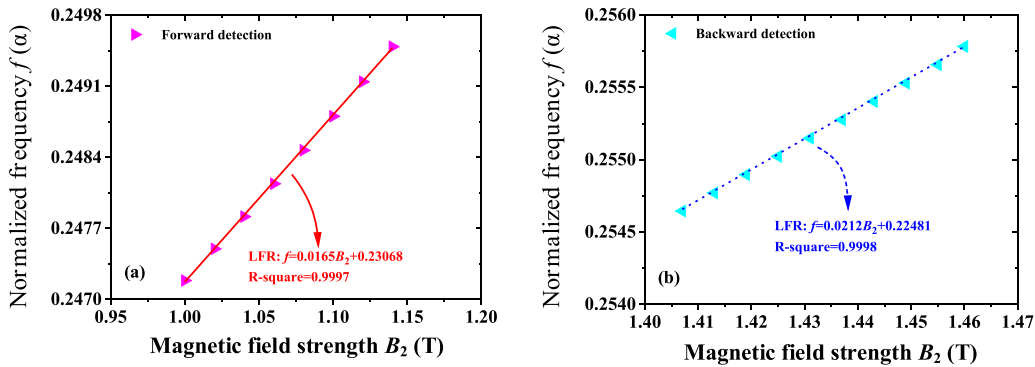

Figure 14. LFR between NAF and magnetic field strength B_2 in the forward and backward sales when both B_1 and B_2 exist. (a) The forward scale. (b) The backward scale.

$B_1 = 1.36$ T. On the contrary, for the figure 10(b), under the condition of $B_1 = 1.411$ T, 1.407 T to 1.46 T are the range of B_2 and 0.254 64 α to 0.255 78 α is a scope of the NAF. The LFR between B_2 and the NAF displays in figure 14 . For the forward detection, under the condition that $B_1 = 1.36$ T, the LFR of B_2 and S are $f = 0.0165B_2 + 0.23068$ and 0.0165 α/T. R-square is 0.9997, when detecting magnetic field strength on the backward scale, under the condition of $B_1 = 1.411$ T, the LFR is $f = 0.0212B_2 + 0.22481$ and S is 0.0212 α/T. The R-square of the LFR is 0.9998. The average values of FOM, Q, and DL are indicated in figures 15(a) and (b). On the forward scale, the relevant values are about 4125 T^{-1}, 62 079, 0.12 $\times$ 10^{-4} T, respectively, and the average A is 0.9767. Oppositely, on the

backward scale, 4240 T^{-1}, 51 041.71, 0.12 $\times$ 10^{-4} T are the correlative values, and A is 0.9757, exceeding 0.9.

To sum up, S, FOM, Q, and DL are the important parameters to evaluate the performance of the detector device. An excellent device owns a higher S, a higher Q, a higher FOM, and a lower DL [33], table 2 indicates the comparison of relative parameters between reported logic gates or sensing detectors and the work of this paper, it follows from this that values of performance gained from the above discussion completely enable to realize a multi-scale magnetic field strength B_1 or B_2 detector. Additionally, the measurement ranges which refer to both the magnetic flux intensity and the NAF exist a large difference when EWs propagate respectively in opposite
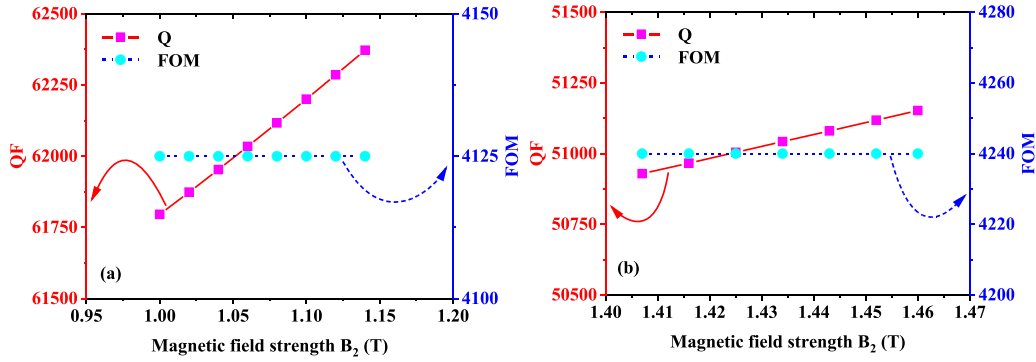
Figure 15. The Q and FOM at different B_2 under the condition of '1 OR 1 = 1'. (a) The forward sensing. (b) The backward sensing.

Table 2. The performance parameters of the proposed PCLT compare with the published studies.

References	Parameter		Performance	Magnetic induction	Logic
[40]	S		6.5 nm T^{-1}	None	None
	Q		7062		
	FOM		6.5 nm T^{-1}		
[41]	S		None	None	OR logic
	Q				XOR logic
	FOM				
[42]	S		None	0.14 T – 0.22 T	None
	Q				
	FOM				
This work	Forward	S	0.0169 α/T	1.19 T – 1.4 T	OR logic
		Q	62372.09		
		FOM	4225		
	Backward	S	0.0225 α/T	1 T – 1.2 T	
		Q	63626.25		
		FOM	5200		

From the above, the logic OR operations '1 OR 0 = 1', '0 OR 1 = 1', '1 OR 1 = 1', '0 OR 0 = 0' can be obtained from the input LLs and APs which have different values (i.e. the determination of the LL displays on the output). As a result, reliable OR logic operations and a large range of magnetic field strength sensing are implemented on forwarding and backward scales.

directions, contributing to distinguishing forward and backward detection. And it leads to significantly increasing the detection range of the entire structure. In the same range, the detection of the magnetic field strength with different precision can be achieved via different DLs.

4. Conclusion

This paper proposes a PCLT that combines two scales of magnetic control OR logic operation and magnetic field sensing. Through the calculation of the transfer matrix method, the *A* of the structure exceeds 0.9. The NAF position of AP can be adjusted by altering the magnetic field. It follows that the logic OR operation can be realized via changing the external magnetic field strength. Additionally, magnetic field sensing which always keeps the function of logic OR operation can be validated by the target sharp AP, the maximum ranges of detection are respectively about 1.19 T – 1.4 T and 1.407 T – 1.46 T on the forward and backward scales. In summary, the

1D magnetized InSb PCLT proposed in this paper has the functions of magnetic control OR logic operation and two-scale sensing, which means that the PCLT has a wide range of potential applications in the fields of biological detection, optical communication, and optical computing.

J. Phys. D: Appl. Phys. **55** (2022) 415001

J Sui *et al*

ORCID iD

Haifeng Zhang ⓘ https://orcid.org/0000-0002-9890-8345

References

[1] Jandieri V, Onoprishvili T and Khomeriki R 2019 *Opt. Quantum Electron.* **51** 1–15
[2] Caballero L P, Povinelli M L and Ramirez J C 2022 *Opt. Express* **30** 1976–93
[3] Chen P, Kong F M and Li K 2008 *Acta Photonica Sin.* **37** 721
[4] Awad M A and Aly A H 2019 *Ceram. Int.* **45** 19036–43
[5] Ali M Z and Abdullah T 2008 *Phys. Lett.* A **372** 1695–700
[6] Alagappan G, Sun X W, Shum P, Yu M B and Doan M T 2006 *J. Opt. Soc. Am.* B **23** 159–67
[7] Abouti O E, Boudouti E, Hassouani Y E, Noual A and Djafari-Rouhani B 2016 *Phys. Plasmas* **23** 082115
[8] Awasthi S K, Panda R and Shiveshwari L 2017 *Phys. Plasmas* **24** 072111
[9] Du G X, Mori T, Suzuki M, Saito S, Fukuda H and Takahashi M 2010 *Appl. Phys. Lett.* **96** 081915
[10] Jia W, Li Y and Xi Y 2003 *J. Phys.: Condens. Matter* **15** 6731
[11] Wang L, Han Y and Huang Y 2013 *IEEE Trans. Instrum. Meas.* **62** 3202–8
[12] Baschirotto A, Dallago E, Malcovati P, Marchesi M and Venchi G 2007 *IEEE Trans. Instrum. Meas.* **56** 25–31
[13] Wei H Y and Wilkinson A J 2011 *IEEE Trans. Instrum. Meas.* **60** 3853–9
[14] Mohr F and Schadt F 2004 *SPIE* **5502** 410–3
[15] Gevorgyan A H 2013 *J. Contemp. Phys.* **48** 75–80
[16] Krause M, Meyne S, Renner H and Brinkmeyer E 2011 *Electron. Lett.* **47** 1392–3
[17] Lin X, Xu Y, Zhang B, Hao R, Chen H and Li E 2013 *New J. Phys.* **15** 113003
[18] Yu M A, Zhang H and Zhang H 2018 *Plasma Sci. Technol.* **21** 015001
[19] Wu Y H and Fang Y T 2019 *Int. J. Mod. Phys.* B **33** 1950034
[20] Rashidi A, Nayak C, Bezerra C G, Costa C H and Pinheiro F A 2020 *Appl. Opt.* **59** 11034–40
[21] Du G X, Mori T and Suzuki M 2010 *Appl. Phys. Lett.* **96** 08191
[22] Chen Z, Zhou Y, Shen J T, Ku P-C and Steel D 2021 *Phys. Rev.* A **103** 052610
[23] Yan D, Li J and Wang Y 2019 *Laser Phys.* **30** 016208
[24] Wu K S, Dong J W, Chen D H, Luo X-N and Wang H-Z 2009 *J. Mod. Opt.* **56** 1895–989
[25] Zhuo L *et al* 2020 *Photonics Res.* **8** 1949–57
[26] Badri S H, Gilarlue M M, Farkoush S G and Rhee S-B 2021 *JOSA* B **38** 1283–9
[27] Badri S H and Farkoush S G 2021 *Appl. Opt.* **60** 2803–10
[28] Youngblood N, Anugrah Y, Ma R, Koester S J and Li M 2014 *Nano Lett.* **14** 2741–6
[29] Shibayama J, Yamahira A, Mugita T, Yamauchi J and Nakano H 2003 *J. Lightwave Technol.* **21** 1709–15
[30] Kazempour B 2019 *Indian J. Phys.* **93** 1369–75
[31] Mauriz P W, Vasconcelos M S and Albuquerque E L 2009 *Phys. Lett.* A **373** 496–500
[32] Wan B F, Xu Y, Zhou Z W, Zhang D and Zhang H F 2020 *IEEE Sens. J.* **21** 2864–2853
[33] Chen S, Fan F, Wang X, Wu P, Zhang H and Chang S 2015 *Opt. Express* **23** 1015–24
[34] Trokhimchuck P P 2008 *Second Int. Conf. on Advanced Optoelectronics and Lasers* vol 7009 p 700906
[35] Xuan L, Kong X, Wu J, He Y and Xu Z 2021 *Appl. Magn. Reson.* **52** 649–60
[36] Qi L, Yang Z, Lan F, Gao X and Shi Z 2010 *Phys. Plasmas* **17** 042501
[37] Chen Z, Zhou Y and Shen J-T 2017 *Opt. Lett.* **42** 887–90
[38] Chen Z, Zhou Y and Shen J-T 2018 *Phys. Rev.* A **98** 053830
[39] Zaky Z A, Ahmed A M, Shalaby A S and Aly A H 2020 *Sci. Rep.* **10** 1–9
[40] Su D, Pu S, Mao L, Wang Z and Qian K 2016 *Sensors* **16** 2157
[41] Kabilan A P, Christina X S and Caroline P E 2010 *2010 2nd Int. Conf. on Computing, Communication and Networking Technologies* (IEEE) pp 1–4
[42] Atalay S, Kaya A O, Kolat V S, Gencer H and Izgi T 2015 *J. Supercond. Nov. Magn.* **28** 2071–5
[43] Ardakani A G 2015 *Eur. Phys. J.* B **88** 1–7